Li XY, Li Z, An GJ, Liu S, Lai YD. Co-expression of perforin and granzyme B genes induces apoptosis and inhibits the tumorigenicity of laryngeal cancer cell line Hep-2. Int J Clin Exp Pathol 2014;7:978–86.

Lima-Junior DS, Costa DL, Carregaro V, Cunha LD, Silva ALN, Mineo TWP, et al. Inflammasome-derived IL-1β production induces nitric oxide-mediated resistance to Leishmania. Nat Med 2013;19:909–15.

Muñoz-Planillo R, Kuffa P, Martínez-Colón G, Smith BL, Rajendiran TM, Núñez G. K^+ efflux is the common trigger of NLRP3 inflammasome activation by bacterial toxins and particulate matter. Immunity 2013;38:1142–53.

Novais FO, Carvalho AM, Clark ML, Carvalho LP, Beiting DP, Brodsky IE, et al. CD8+T cell cytotoxicity mediates pathology in the skin by inflammasome activation and IL-1β production. PLoS Pathog 2017;13:e1006196.

Novais FO, Carvalho LP, Passos S, Roos DS, Carvalho EM, Scott P, et al. Genomic profiling of human *Leishmania braziliensis* lesions identifies transcriptional modules associated with cutaneous immunopathology. J Invest Dermatol 2015;135:94–101.

Place DE, Kanneganti TD. Recent advances in inflammasome biology. Curr Opin Immunol 2018;50:32–8.

Santos CDS, Boaventura V, Ribeiro Cardoso C, Tavares N, Lordelo MJ, Noronha A, et al. CD8(+) granzyme B(+) -mediated tissue injury vs. CD4(+)IFNγ(+)-mediated parasite killing in human cutaneous leishmaniasis. J Invest Dermatol 2013;133:1533–40.

Santos D, Campos TM, Saldanha M, Oliveira SC, Nascimento M, Zamboni DS, et al. IL-1β production by intermediate monocytes is associated with immunopathology in cutaneous leishmaniasis [published correction appears in J Invest Dermatol 2014 Nov;134(11):2850]. J Invest Dermatol 2018;138:1107–15.

Diagnostic Two-Gene Classifier in Early-Stage Mycosis Fungoides: A Retrospective Multicenter Study

Journal of Investigative Dermatology (2021) **141,** 213–217; doi:10.1016/j.jid.2020.04.026

TO THE EDITOR

Although mycosis fungoides (MF) is the most common cutaneous T-cell lymphoma, it still poses a major diagnostic challenge because of clinical and histological similarities to benign inflammatory dermatosis (BID), resulting in prolonged diagnostic workup (Scarisbrick et al., 2019). Algorithms based on clinical, morphological, immunophenotypical, and molecular parameters have added to diagnostic accuracy in early-stage disease (Pimpinelli et al., 2005). In addition, *TOX*, *PDCD1*, *CADM1*, *BLK*, and genes related to the TNF signaling pathway have been reported as potential diagnostic markers (Krejsgaard et al., 2009; Litvinov et al., 2017; Tracey et al., 2003; Yuki et al., 2018; Zhang et al., 2012). Decades of research have provided considerable evidence on the interaction between malignant T cells and benign immune and stromal cells, inhibiting antitumor responses while promoting tumor cell growth through the inflammatory microenvironment produced by the neoplastic cells and thereby driving the stage-related inflammation characteristic of MF (Krejsgaard et al., 2017). Only a few studies have investigated the role of the innate immune cells (Cioplea et al., 2019). To this end, we performed gene expression analysis with emphasis on the innate immune system on 43 initial diagnostic biopsies from 36 patients with early-MF ($\leq$ IIA) and 47 controls (13 healthy skin, 35 BID) (Supplementary Table S1) using the NanoString nCounter Human Myeloid Innate Immunity Panel v2 spiked with 30 customized genes (Supplementary Materials and Methods; Supplementary Table S2). Patients were included using conventional clinical and histopathological criteria. Patient consent for experiments was not required because retrospective studies are exempted according to Danish laws. Based on the 535 most differentially expressed genes ($\sigma/\sigma_{max} > 0.2$), an overall good separation of early-stage MF (early-MF), BID, and healthy skin was observed (Supplementary Figure S1a), and a direct comparison of early-MF and BID (*t*-test: fold change > 3 and $P < 0.01$) identified 45 differentially expressed genes, of which all except one (*SAA1*) were highly expressed in early-MF compared with BID. Based on these genes, a semi-unsupervised two-way hierarchical clustering revealed almost complete separation of early-MF from BID (Supplementary Figure S1b). To build a minimal diagnostic classifier for early-MF, we tested different combinations of the 45 differentially expressed genes to identify the combination that gave the best classifier performance by 10-fold cross-validation. The final classifier consisted of the two genes *TOX* and *TRAF1* (Figure 1a) with a classification accuracy of 90% (Figure 1c). This two-gene classifier was evaluated in an independent validation cohort of 27 patients with early-MF and 17 patients with BID (Figure 1b), with a classification accuracy of 80% (Figure 1d).

Automated digital quantification of protein expression of TOX and TRAF1 revealed a significant upregulation of both TOX and TRAF1 proteins in early-MF compared with controls ($P < 0.0001$ and $P < 0.0001$, respectively) (Figure 2a and b). TOX protein expression was seen in benign lymphocytes in controls and MF, as well as neoplastic lymphocytes in MF located in Pautrier micro-abscesses and dermis (Figure 2c and d). Previous studies report putative diagnostic and prognostic roles for TOX in MF (Huang et al., 2014; Litvinov et al., 2017; Zhang et al., 2012); however, the diagnostic potential has been questioned as TOX expression is not restricted to $CD4^+$ cells (Schrader et al.,

Abbreviations: BID, benign inflammatory dermatosis; early-MF, early-stage mycosis fungoides; MF, mycosis fungoides

Accepted manuscript published online 23 May 2020; corrected proof published online 15 July 2020

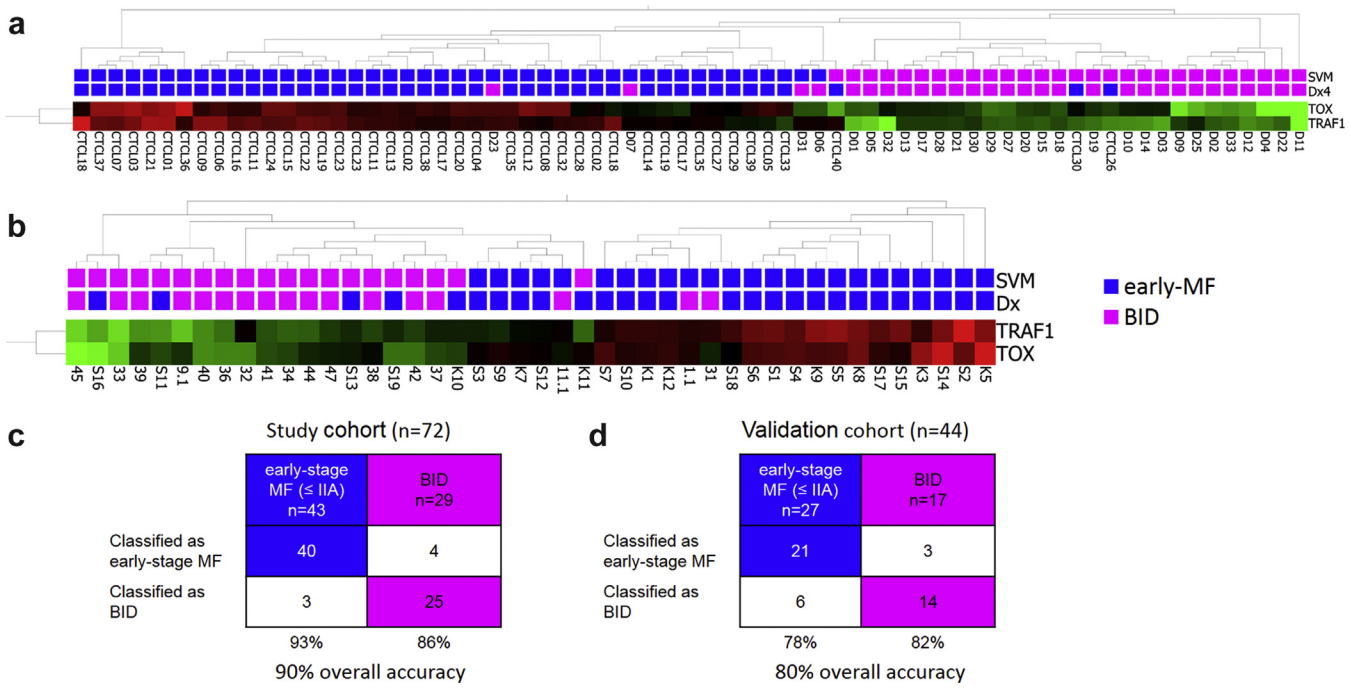

Figure 1. Two-gene diagnostic classifier in early-MF. (**a**) Minimal SVM classifier trained on combinations of the top 45 DEGs between early-MF (n = 43) and BID (n = 29) in the study cohort. (**b**) The trained SVM classifier applied on early-MF (n = 27) and BID (n = 17) in an independent validation cohort. (**c**) Classification performance in the study cohort of the SVM two-gene classifier with a sensitivity and specificity of 93% and 86%, respectively. (**d**) Classification performance in the validation cohort of the classifier with a sensitivity and specificity of 78% and 82%, respectively. BID, benign inflammatory dermatosis; DEG, differentially expressed gene; early-MF, early-stage mycosis fungoides; MF, mycosis fungoides; SVM, support vector machine.

2016). Our data confirm these findings by showing that TOX mRNA and protein expression was highly upregulated in early-MF compared with BID. There was, however, a substantial overlap between MF and BID lesions, stressing that TOX positivity at the single-patient level was not sufficient to classify individual samples. TRAF1 protein expression was seen in scattered benign lymphocytes in MF and controls. In MF, TRAF1 positivity was also identified in cells with a dendritic morphology in Pautrier micro-abscesses in close proximity with TRAF1-positive neoplastic T cells and in dermal aggregates resembling dendritic networks (Figure 2f). To identify the cellular origin of the dendritic cells, double immunofluorescence was performed (Figure 2g–k). TRAF1 was expressed in T cells, especially in the neoplastic lymphocytes in the Pautrier micro-abscesses (Figure 2g), and in a subpopulation of dendritic cells with an immature phenotype (Langerin$^+$, CD11c$^+$, and CD1a$^+$; Figure 2h, i, and k). Furthermore, TRAF1 was expressed in scattered S100$^+$ Langerhans cells (Figure 2j), and there was a large population of double immunofluorescence TRAF1-negative dendritic cells, which was increased in early-MF compared with BID. No macrophages (CD68$^+$ or CD163$^+$) or B cells were TRAF1-positive (data not shown). We saw that TRAF1 was intensely expressed in neoplastic T cells and immature dendritic cells in tumor-stage MF, and the TRAF1-negative population of immature dendritic cells was also increased with disease progression (data not shown).

The major source of TRAF1 expression in our study was S100- or Langerin-positive dendritic cells accumulating in the epidermis and upper dermis in early-MF compared with controls. Similar findings have been reported previously (Der-Petrossian et al., 2011; Lüftl et al., 2002), and likewise we found small populations of immature CD1a$^+$/CD11c$^+$ and TRAF1-positive cells in early-MF that increased with disease progression in concordance with other studies (Cioplea et al., 2019; Schlapbach et al., 2010). It has been proposed that immature dendritic cells may play a critical role in stimulating the growth of tumor cells in cutaneous T-cell lymphoma (Berger et al., 2002), and blocking the maturation of these cells with IL-10 demonstrates a down-regulation of antitumor immunity (Lüftl et al., 2002; Steinbrink et al., 1999).

In this study, we have identified and validated a diagnostic classifier based on the two genes *TOX* and *TRAF1* with a potential ability to distinguish between early-MF and BID. Limitations of this study include the low number of study subjects; restricted analyses to myeloid cells and, to a lesser extent, related to genes from the adaptive immune system; and lack of information regarding interaction between inflammatory cells, keratinocytes, and stromal cells. This notwithstanding, we hypothesize that the combination of *TOX* and *TRAF1* can prove to be valuable diagnostic markers in early-MF, and we believe that the addition of other markers will increase overall diagnostic accuracy. Furthermore, *TOX* and *TRAF1* may present novel therapeutic targets in MF.

Data availability statement

Datasets related to this article have been deposited in the Gene Expression Omnibus, with accession number GSE143382.

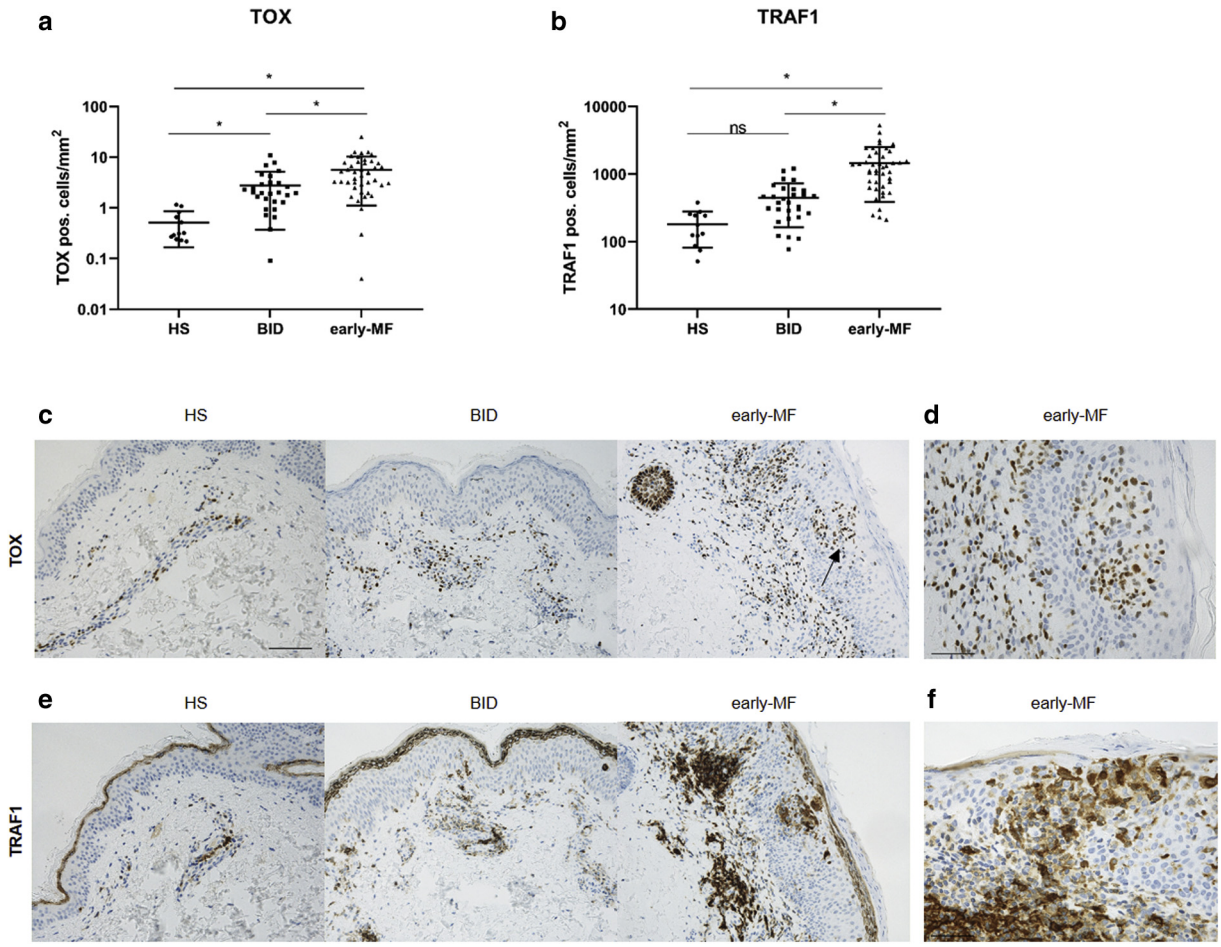

Figure 2. IHC, immunofluorescence staining, and digital assessment of TOX and TRAF1 proteins in early-MF, BID, and HS. (**a, b**) Scatter plots of IHC staining and digital analysis (Leica Tissue IA 2.0 software) of (**a**) TOX and (**b**) TRAF1 in percent positive cells per mm^2. A two-fold increase of TOX-positive cells/mm^2 was seen in early-MF compared with BID or HS (5.7 ± 4.6 vs. 2.8 ± 2.4, $P < 0.0001$). Mean TOX-positive cells/mm^2 in HS was 0.5 ± 0.3, which was significantly lower than in early-MF ($P < 0.0001$) and BID ($P = 0.02$). (**b**) An almost 3-fold increase of TRAF-positive cells was seen in early-MF compared with BID (1,447 ± 1,059 vs 446.2 ± 282.8 TRAF1-positive cells/mm^2, $P < 0.0001$). The mean number of TRAF1-positive cells/mm^2 in HS was 180.9 ± 99.5, which was significantly lower than early-MF ($P < 0.0001$). No significant difference was detected between HS and BID ($P = 0.09$). Horizontal lines represent means ± SD, *$P < 0.05$ by the nonparametric Kruskal-Wallis test. (**c**) IHC of TOX in HS, BID, and early-MF showing a few scattered and weakly stained dermal lymphocytes in HS and BID. In MF, lymphocytes expressed TOX much stronger. The arrow indicates TOX-positive lymphocytes in a Pautrier micro-abscess. Bar = 100 μm. (**d**) High-power image of TOX in the same biopsy. Bar = 50 μm. (**e**) IHC of TRAF1 protein in HS, BID, and early-MF showing a marked upregulation of TRAF1-positive cells in early-MF compared with HS and BID. Bar = 100 μm. (**f**) High-power image of TRAF1 in the same biopsy. Bar = 50 μm. (**g**–**k**) Cellular origin of TRAF1-positive dendritic cells was examined by dIF staining. Co-expression of TRAF1 was investigated with (**g**) CD3, (**h**) CD1a, (**i**) CD11c, (**j**) S100, or (**k**) Langerin. Single-stained cells are either red (TRAF1), green (protein of interest), or yellow (double positive). Cells are detected in Pautrier micro-abscesses or in dermal infiltrates. The DAPI stain (right column) was used to visualize the nuclei of cells. Original magnification for all, ×40. Bar = 50 μm. BID, benign inflammatory dermatosis; dIF, double immunofluorescence; early-MF, early-stage mycosis fungoides; HS, healthy skin; IHC, immunohistochemistry; MF, mycosis fungoides.

ORCIDs
Pia Rude Nielsen: https://orcid.org/0000-0002-7797-3949
Jens Ole Eriksen: https://orcid.org/0000-0002-8846-5018
Lise Maria Lindahl: https://orcid.org/0000-0003-3768-4146
Ulrike Wehkamp: https://orcid.org/0000-0002-7398-4261
Michael Bzorek: https://orcid.org/0000-0002-9493-5856
Gitte Andersen: https://orcid.org/0000-0002-1948-6026
Anders Woetmann: https://orcid.org/0000-0002-3008-735X
Lars Iversen: https://orcid.org/0000-0003-1816-4508
Niels Ødum: https://orcid.org/0000-0003-3135-5624
Thomas Litman: https://orcid.org/0000-0002-6068-901X
Lise Mette Rahbek Gjerdrum: https://orcid.org/0000-0003-4377-3209

CONFLICT OF INTEREST
TL is employed both by Copenhagen University and by LEO Pharma A/S. GA receives financial support for research projects from Hologic and holds stock in Novo Nordisk. NØ has received advisory consultant honoraria from Micreos Human Health B.V. LMRG received funding from NanoString Technologies. The remaining authors state no conflict of interest.

ACKNOWLEDGMENTS
The invaluable technical assistance by the immunohistochemical and molecular team at the Department of Pathology (Næstved, Denmark) is highly appreciated. The authors would also like to thank medical doctor Louise Baandrup for collecting healthy skin biopsies.

Preliminary data has been presented in an abstract at the European Organization for Research and Treatment of Cancer Cutaneous Lymphoma Meeting 2019 and at the 61st American Society of Hematology Annual Meeting 2019.

This study was supported by grants from Region Zealand Health and Research Foundation, Aage Bangs Foundation, the Harboe Foundation, the

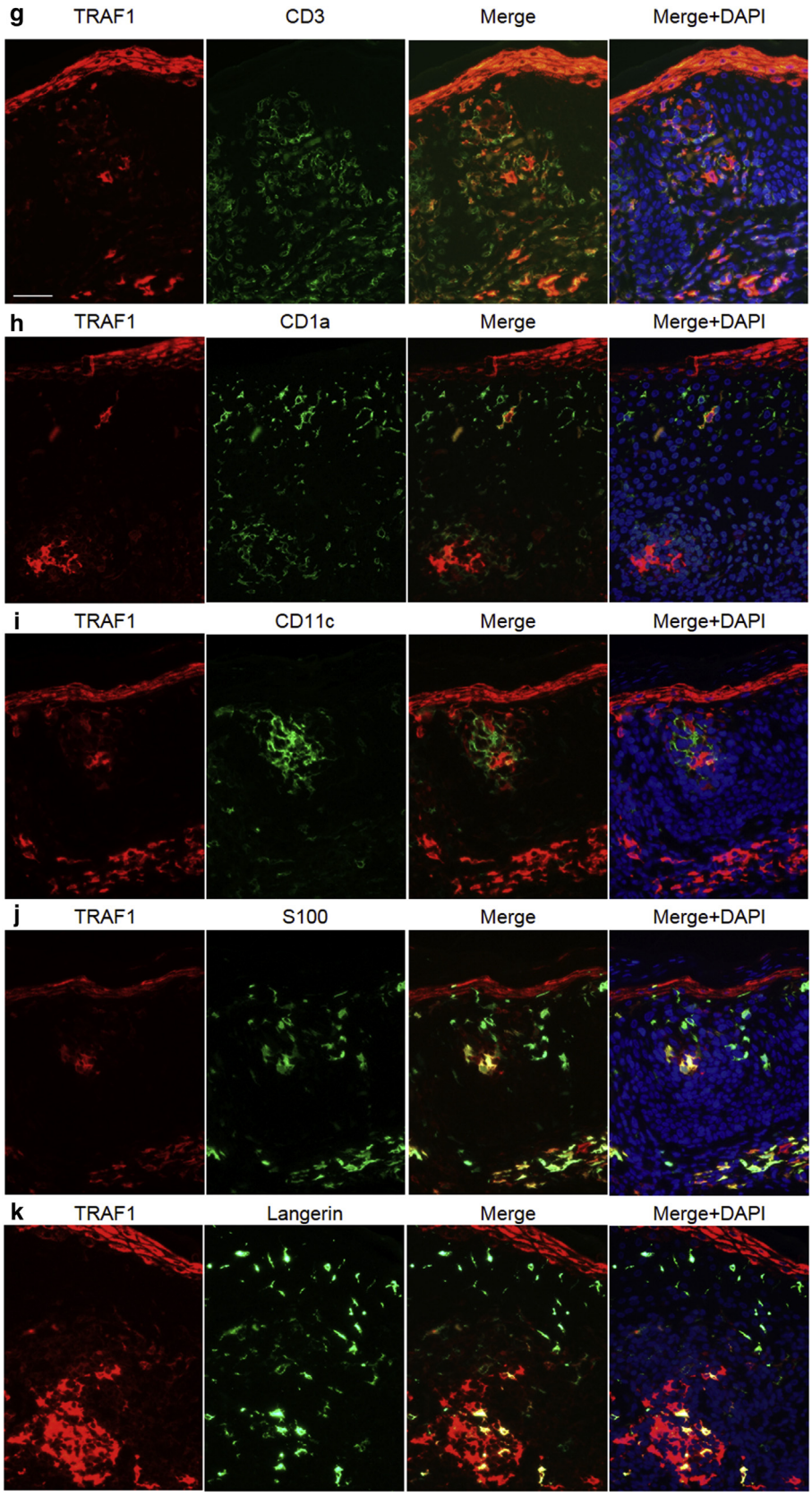

Figure 2. (*continued*)

Danish Cancer Research Foundation (Dansk Kræftforskningsfond), the carpenter Jørgen Holm and wife Elisa F. Hansen Memorial Foundation, the Medical Research Association Foundation, and the A.P. Moeller Foundation.

AUTHOR CONTRIBUTIONS

Conceptualization: LMRG, PRN; Data Curation: PRN, LMRG, LI, LML, UW; Formal Analysis: JOE, PRN, LML, GA, TL, NØ, LMRG, MB; Methodology: NØ, TL, LMRG, JOE, MB, AW, PRN; Writing - Original Draft Preparation: PRN, LMRG, JOE, MB, TL; Writing - Review and Editing: PRN, JOE, LML, UW, MB, GA, AW, LI, NØ, TL, LMRG

***Pia Rude Nielsen*[1,2], *Jens Ole Eriksen*[1], *Lise Maria Lindahl*[3], *Ulrike Wehkamp*[4], *Michael Bzorek*[1], *Gitte Andersen*[1], *Anders Woetmann*[2], *Lars Iversen*[3], *Niels Ødum*[2], *Thomas Litman*[2] and *Lise Mette Rahbek Gjerdrum*[1,5,*]**

[1]*Department of Pathology, Zealand University Hospital, Denmark;* [2]*Leo Foundation Skin Immunology Research Center, Department of Immunology and Microbiology, University of Copenhagen, Denmark;* [3]*Department of Dermatology, Aarhus University Hospital, Aarhus, Denmark;* [4]*Department of Dermatology, University Hospital, Schleswig-Holstein, Kiel, Germany; and* [5]*Department of Clinical Medicine, University of Copenhagen, Denmark*

[*]*Corresponding author e-mail: lmgj@regionsjaelland.dk*

SUPPLEMENTARY MATERIAL

Supplementary material is linked to the online version of the paper at www.jidonline.org, and at https://doi.org/10.1016/j.jid.2020.04.026.

REFERENCES

Berger CL, Hanlon D, Kanada D, Dhodapkar M, Lombillo V, Wang N, et al. The growth of cutaneous T-cell lymphoma is stimulated by immature dendritic cells. Blood 2002;99:2929–39.

Cioplea M, Caruntu C, Zurac S, Bastian A, Sticlaru L, Cioroianu A, et al. Dendritic cell distribution in mycosis fungoides vs. inflammatory dermatosis and other T-cell skin lymphoma. Oncol Lett 2019;17:4055–9.

Der-Petrossian M, Valencak J, Jonak C, Klosner G, Dani T, Müllauer L, et al. Dermal infiltrates of cutaneous T-cell lymphomas with epidermotropism but not other cutaneous lymphomas are abundant with langerin$^+$ dendritic cells. J Eur Acad Dermatol Venereol 2011;25:922–7.

Huang Y, Litvinov IV, Wang Y, Su MW, Tu P, Jiang X, et al. Thymocyte selection-associated high mobility group box gene (TOX) is aberrantly over-expressed in mycosis fungoides and correlates with poor prognosis. Oncotarget 2014;5:4418–25.

Krejsgaard T, Lindahl LM, Mongan NP, Wasik MA, Litvinov IV, Iversen L, et al. Malignant inflammation in cutaneous T-cell lymphoma-a hostile takeover. Semin Immunopathol 2017;39:269–82.

Krejsgaard T, Vetter-Kauczok CS, Woetmann A, Kneitz H, Eriksen KW, Lovato P, et al. Ectopic expression of B-lymphoid kinase in cutaneous T-cell lymphoma. Blood 2009;113:5896–904.

Litvinov IV, Tetzlaff MT, Thibault P, Gangar P, Moreau L, Watters AK, et al. Gene expression analysis in cutaneous T-cell lymphomas (CTCL) highlights disease heterogeneity and potential diagnostic and prognostic indicators. Oncoimmunology 2017;6:e1306618.

Lüftl M, Feng A, Licha E, Schuler G. Dendritic cells and apoptosis in mycosis fungoides. Br J Dermatol 2002;147:1171–9.

Pimpinelli N, Olsen EA, Santucci M, Vonderheid E, Haeffner AC, Stevens S, et al. Defining early mycosis fungoides. J Am Acad Dermatol 2005;53:1053–63.

Scarisbrick JJ, Quaglino P, Prince HM, Papadavid E, Hodak E, Bagot M, et al. The PROCLIPI international registry of early-stage mycosis fungoides identifies substantial diagnostic delay in most patients. Br J Dermatol 2019;181:350–7.

Schlapbach C, Ochsenbein A, Kaelin U, Hassan AS, Hunger RE, Yawalkar N. High numbers of DC-SIGN+ dendritic cells in lesional skin of cutaneous T-cell lymphoma. J Am Acad Dermatol 2010;62:995–1004.

Schrader AMR, Jansen PM, Willemze R. TOX expression in cutaneous T-cell lymphomas: an adjunctive diagnostic marker that is not tumour specific and not restricted to the CD4(+) CD8(−) phenotype. Br J Dermatol 2016;175:382–6.

Steinbrink K, Jonuleit H, Müller G, Schuler G, Knop J, Enk AH. Interleukin-10-treated human dendritic cells induce a melanoma-antigen-specific anergy in CD8(+) T cells resulting in a failure to lyse tumor cells. Blood 1999;93:1634–42.

Tracey L, Villuendas R, Dotor AM, Spiteri I, Ortiz P, García JF, et al. Mycosis fungoides shows concurrent deregulation of multiple genes involved in the TNF signaling pathway: an expression profile study. Blood 2003;102:1042–50.

Yuki A, Shinkuma S, Hayashi R, Fujikawa H, Kato T, Homma E, et al. CADM1 is a diagnostic marker in early-stage mycosis fungoides: multicenter study of 58 cases. J Am Acad Dermatol 2018;79:1039–46.

Zhang Y, Wang Y, Yu R, Huang Y, Su M, Xiao C, et al. Molecular markers of early-stage mycosis fungoides. J Invest Dermatol 2012;132:1698–706.

Screening Novel Agent Combinations to Expedite CTCL Therapeutic Development

Journal of Investigative Dermatology (2021) **141,** 217–221; doi:10.1016/j.jid.2020.05.097

TO THE EDITOR

Cutaneous T-cell lymphoma (CTCL) is a group of non-Hodgkin lymphomas of skin-homing malignant T lymphocytes. In advanced stages, CTCL is incurable and often fatal (Arulogun et al., 2008), and blood involvement portends a poorer outcome (Agar et al., 2010). Overall response rates to systemic therapies are 30–50% and generally not durable. High-throughput screening has emerged as a rapid method for identification and prioritization of novel therapeutic compounds. Analysis of natural compounds and agents in ongoing clinical trials may accelerate opportunities for drug repurposing, synergy testing, and preclinical assessment for CTCL therapeutic potential.

Patients with CTCL at the Yale Cancer Center (New Haven, CT) were enrolled with written and informed consent in accordance with the Yale Human Investigational Review Board. For initial screening, malignant cells were isolated from the peripheral blood of four patients with CTCL, as previously reported (Cyrenne et al., 2017; Kim et al., 2018). High-throughput screening was conducted on a 1,348 agent panel rich in phosphatase and kinase inhibitors and natural compounds (Selleckchem Kinase Inhibitors, Enzo Phosphatase Inhibitors, and MicroSource Gen-Plus libraries) at the Yale Center for Molecular Discovery (New Haven, CT). The 4,000–6,000

Abbreviations: CTCL, cutaneous T-cell lymphoma

Accepted manuscript published online 12 June 2020; corrected proof published online 14 July 2020

SUPPLEMENTARY MATERIALS AND METHODS

Patients and study material

The study cohort consists of 36 patients with early-stage mycosis fungoides (early-MF) (stage ≤IIA), from whom 43 formalin-fixed and paraffin embedded (FFPE) skin biopsies were obtained. Controls included 12 biopsies from healthy skin and 29 biopsies from patients with benign inflammatory dermatosis (BID; dermatitis in all cases). Seven patients had two longitudinal biopsies with early-MF available for analysis. All samples in the study cohort were collected from the archives at the Department of Pathology, Zealand University Hospital, Denmark as previously described (Nielsen et al., 2019). An independent validation cohort of 27 FFPE skin samples from patients with early-MF was provided by the Department of Dermatology, Aarhus University Hospital, Denmark and the Department of Dermatology, University Hospital, Schleswig-Holstein, Kiel, Germany. All histological slides and clinical records were reviewed for establishing the diagnosis according to the International Society for Cutaneous Lymphomas and European Organization of Research and Treatment of Cancer recommendations (Olsen et al., 2007). Clinical characteristics such as age, sex, clinical stage at the time of diagnosis, disease progression, treatment, and follow-up time were registered for each patient. The study was approved by the local ethical committees (SJ-603, 1-10-72-91-13, and B249/16) and the Data Protection Agency (J.NR. REG-009-2017).

RNA isolation and quantification

Total RNA was isolated from ten 10-μm sections of FFPE samples from HS, BID, and early-MF using the Roche high pure RNA FFPE isolation kit (Roche, Basel, Switzerland) according to the manufacturer's guidelines. Total RNA quality and quantity were measured by Nanodrop Lite spectrophotometer (Thermo Fisher Scientific, Waltham, MA).

Gene expression analysis

From each FFPE sample, 50−100 ng of RNA was used for the gene expression analysis of 770 genes related to the innate immune system with the nCounter Human Myeloid Innate Immunity Panel v2 utilizing the NanoString platform (NanoString Technologies, Seattle, WA) using the CodeSet-Plus/Panel-Plus nCounter XT Gene Expression Assay. A total of 30 additional genes of interest were added to the panel (Supplementary Table S2). Raw data were quality checked in the nSolver software by using the default parameters; in this process, imaging QC, binding density, positive control linearity, and positive control limit of detection (set to 0.5 fM) was evaluated. Background subtraction was done with negative control thresholding using the average of the included negative controls. Normalization factors were calculated based on the 40 housekeeping genes included in the myeloid innate immunity panel.

Protein analysis using immunohistochemical staining

Immunohistochemical staining of TOX and TRAF1 was performed on all patients included in the study cohort (early-MF, BID, and HS). FFPE sections (3-μm thick) were stained on the fully automated instrument Omnis (Dako, Carpinteria, CA). Sections were deparaffinized and exposed to antigen retrieval using EnVision FLEX Target Retrieval Solution (3-in-1) pH 9 (Dako) and heated for 24 minutes at 97 °C. Slides were incubated with primary antibodies against TOX (Sigma-Aldrich, St. Louis, MO, cat #HPA018322) and TRAF1 (Cell Signaling Technology, Danvers, MA, cat #4715) at a dilution of 1:200 and 1:50, respectively. Antibodies were diluted in Renoir Red (Biocare Medical, Pacheco, CA, cat #PD904L). After washing and blocking of endogenous peroxidase activity, the reactions were detected and visualized using Envision FLEX+ High pH kit (Dako) according to the manufacturer's instructions. Finally, slides were rinsed in water, counterstained with Mayer's hematoxylin, and mounted with Pertex. Tonsillar tissue was used as positive and negative controls for each antibody.

Immunohistochemical assessment of TOX- and TRAF1-positive cells

The immunostained slides for TOX and TRAF1 were scanned in a Leica SCN400 slide scanner (Leica Microsystems, Wetzlar, Germany) at ×20. All files of the scanned slides were transferred to the Digital Image Hub server software (Slidepath/Leica Microsystems) provided with image analysis plug-in TissueIA 2.0 software. Algorithms for the individual immunostains were developed separately and were based on the detection of TOX (nuclear localization and deconvolution DAB/deconvolution hematoxylin) and TRAF1 (cytoplasmic localization and deconvolution DAB/deconvolution hematoxylin) reactions. The algorithms were adjusted to the strength of the hematoxylin nuclear counterstain and the size of both the cell and nucleus as well as cell density. Owing to the relatively small tissue area of the skin biopsies, and because both TOX- and TRAF1-positive cells were present in the epidermal and dermal compartments, the algorithms were applied to the whole tissue area. The results were presented as percent positive cells per area in mm^2 for both biomarkers. The ability of the algorithms to detect and quantitate the biomarkers were adjusted iteratively and finally confirmed in close collaboration between the software operator and an expert pathologist.

Double immunofluorescence staining

For subtyping TRAF1-positive cells, double immunofluorescence labeling (simultaneous technique) was applied on representative cases of early-MF, BID, HS, and tumor MF. TRAF1 was used in combination with either CD3, CD20, CD1a, CD14, CD11c, CD68, CD163, S100, or Langerin antibodies. The double immunofluorescence experiments were performed as described in detail elsewhere with a few modifications (Bzorek et al., 2008). In brief, following deparaffinization and antigen retrieval in Target Retrieval Solution pH 9 for 24 minutes at 97 °C, the slides were incubated with a mixture of rabbit (TRAF1) and mouse (all CD markers, S100, and Langerin) mAbs diluted in Renoir Red for 60 minutes at 32 °C. The reactions were detected with a mix of goat anti-rabbit conjugated with Alexa Fluor 594 (Invitrogen, Carlsbad, CA, cat #A11012) diluted 1:400 and goat anti-mouse conjugated with Alexa Fluor 488 (Invitrogen, cat #A11001) diluted 1:200 in Envision FLEX Antibody Diluent (Dako, cat #K8006) and

incubated for 60 minutes at 32 °C in the dark. After washing and dehydration, slides were air-dried and mounted with Vectashield with DAPI (Vector Laboratories, Burlingame, CA, cat #H-1200). Negative controls were treated with a mixture of Alexa Fluor–conjugated secondary antibodies with omission of the primary antibodies. Slides were evaluated with a Nikon Eclipse 80 fluorescence microscope with standard filter sets for each fluorochrome. FITC (Alexa Fluor 488); Texas Red (Alexa Fluor 594); double filter FITC and Texas Red (Alexa Fluor 488 and Alexa Fluor 594); and triple filter FITC, Texas Red, and DAPI (Alexa Fluor 488, Alexa Fluor 594, and DAPI). Images were captured with a Nikon camera (DS-5Mc Color Cooled Digital/MQA15000). If necessary, brightness and contrast was adjusted with the provided software of the camera.

Data and statistical analysis

Differentially expressed genes were identified by ANOVA (cut-off: variance filter: $\sigma/\sigma max > 0.2$, 2-fold change, and $P < 0.05$), and significance was adjusted for multiple testing by estimating false discovery rates. Data were analyzed and visualized in Qlucore Omics Explorer v. 3.5 (Qlucore AB, Lund, Sweden), including principal component analysis, heat maps, unsupervised hierarchical clustering, and building of classifiers (supervised models).

For development of a diagnostic classifier able to separate early-MF from BID samples, three different methods were tested: κ-nearest neighbors, random trees, and support vector machine, where the latter method performed the best, after optimization of the support vector machine parameters to a radial kernel and gamma = 0.9. The classifier was trained on the study cohort (43 early-MF and 29 BID samples) and validated in an independent cohort (27 early-MF and 17 BID samples). The results of immunohistochemical assessment of TOX and TRAF1 were analyzed in GraphPad Prism (version 8.1.1, GraphPad Software, San Diego, USA) by the nonparametric Kruskal-Wallis test. A significance level of 5% ($\alpha = 0.05$) was considered statistically significant.

SUPPLEMENTARY REFERENCES

Bzorek M, Stamp IM, Petersen BL, Frederiksen L. Use of commercially available rabbit monoclonal antibodies for immunofluorescence double staining. Appl Immunohistochem Mol Morphol 2008;16:387–92.

Nielsen PR, Eriksen JO, Wehkamp U, Lindahl LM, Gniadecki R, Fogh H, et al. Clinical and histological characteristics of mycosis fungoides and Sézary syndrome: a retrospective, single-centre study of 43 patients from Eastern Denmark. Acta Derm Venereol 2019;99:1231–6.

Olsen E, Vonderheid E, Pimpinelli N, Willemze R, Kim Y, Knobler R, et al. Revisions to the staging and classification of mycosis fungoides and Sezary syndrome: a proposal of the International Society for Cutaneous Lymphomas (ISCL) and the Cutaneous Lymphoma Task Force of the European Organization of Research and Treatment of Cancer (EORTC). Blood 2007;110:1713–22.

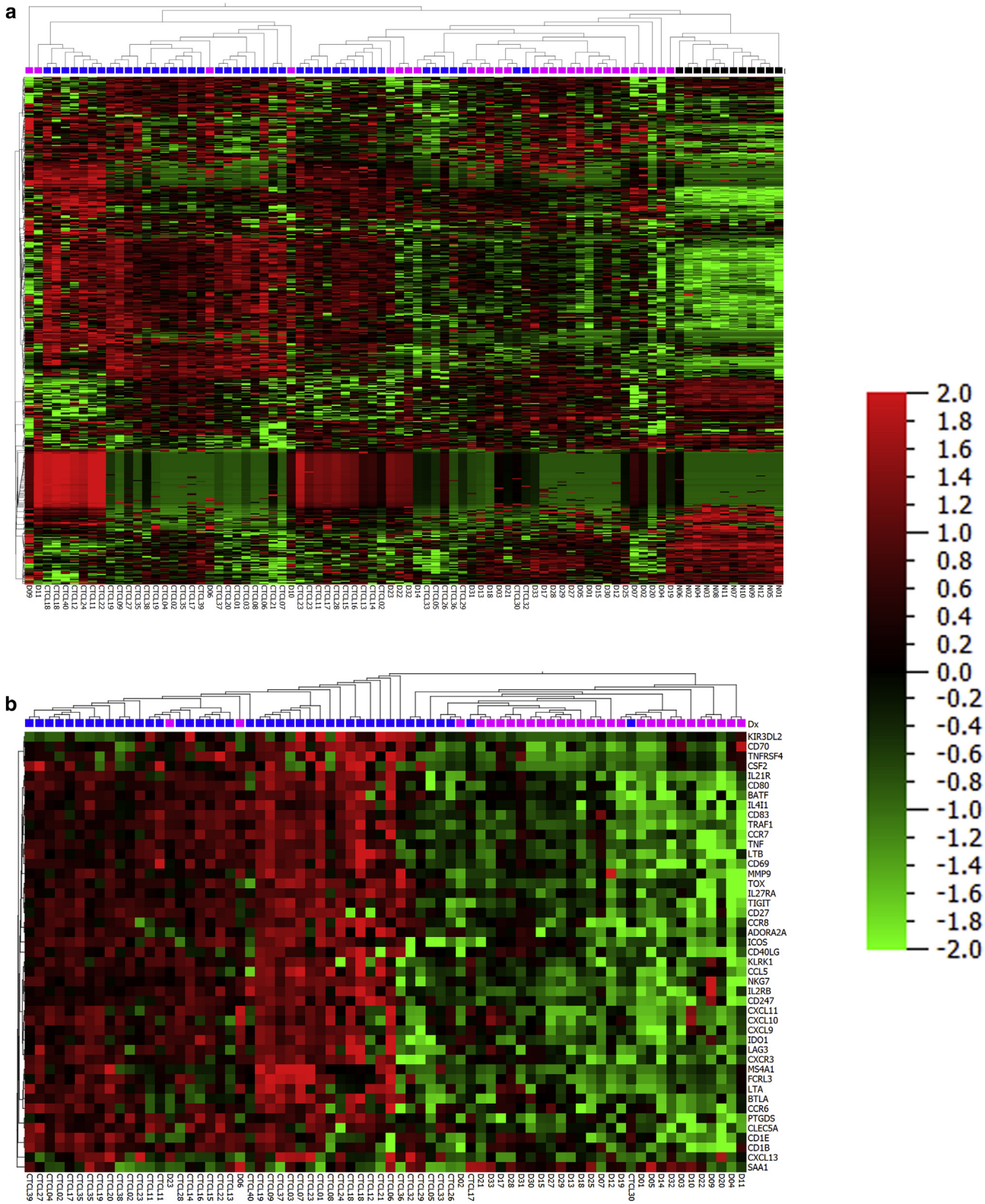

Supplementary Figure S1. (**a**) Heat-map and two-way unsupervised hierarchical clustering based on the 535 most variable genes ($\sigma/\sigma max>0.2$) across all samples, including healthy skin (HS) (n=12), benign inflammatory dermatitis (BID) (n=29) and early-stage MF (early-MF) (n=43). (**b**) Heat-map and two-way hierarchical clustering based on the top 45 differentially expressed genes (>3-fold change, $p<0.01$) between early-MF and BID.The diagnosis (Dx) is indicated above the heatmap (black, HS; pink, BID; blue, early-MF). Samples appear in columns, genes in rows. Gene expression values are z-scaled (mean=0, Var=1) and depicted as nuances of red (higher than the average across samples) or green (lower than the average across samples) as indicated on the color bar.

Supplementary Table S1. Characteristics of Patients with Mycosis Fungoides in the Study Cohort and the Independent Validation Cohort

Patient Characteristics	Study Cohort n = 36 (%)	Independent Validation Cohort n = 27 (%)
Sex		
Male	20 (55.6)	19 (70.4)
Female	16 (44.4)	8 (29.6)
Age		
≤ 60	10 (27.8)	8 (29.6)
> 60	26 (72.2)	19 (70.4)
Clinical stage		
IA	18 (50.0)	19 (70.4)
IB	14 (38.9)	7 (25.9)
IIA		1 (3,7)
ND	4 (11.1)	
T-stage		
T1	18 (50.0)	20 (74.1)
T2	14 (38.9)	7 (25.9)
ND	4 (11.1)	
Treatment[1]		
No treatment	4 (11.1)	7 (25.9)
Topical steroids	14 (38.9)	17 (63.0)
Other[2]	2 (5.6)	3 (11.1)
ND	16 (44.4)	
Progression		
Yes	18 (50.0)	6 (22.2)
No	18 (50.0)	21 (77.8)

Abbreviation: ND, no data.
[1]Treatment at time of biopsy.
[2]Other treatment modalities includes UVB, psoralen plus UVA, nitrogen mustard, methotrexate, and acitretin.

Supplementary Table S2. 30 Customized Genes Supplemented to the nCounter Human Myeloid Innate Immunity Panel v2

Gene	Identifier
AHR	NM_001621.3
CD207	NM_015717.2
CD4	NM_000616.4
CD52	NM_001803.2
DNM3	NM_015569.3
EZH2	NM_001203247.1
FCRL3	NM_052939.3
FOXO1	NM_002015.3
FOXP3	NM_014009.3
HDAC1	NM_004964.2
HDAC9	NM_014707.1
IKZF2	NM_001079526.1
IL13RA1	NM_001560.2
IL17A	NM_002190.2
IL17B	NM_014443.2
IL17F	NM_052872.3
IL17RB	NM_018725.3
IL17RC	NM_153461.2
IL21	NM_021803.2
IL23R	NM_144701.2
IL2RA	NM_000417.1
IL2RB	NM_000878.2
IL7R	NM_002185.2
KIR3DL2	NM_006737.2
NOTCH1	NM_017617.3
BOB1	NM_006235.2
SATB1	NM_001131010.1
TNFSF11	NM_003701.2
TOX	NM_014729.2
TWIST1	NM_000474.3